# Carbon/$MoO_2$ Composite Based on Porous Semi-Graphitized Nanorod Assemblies from In Situ Reaction of Tri-Block Polymers

Xiulei Ji, P. Subramanya Herle, Youngho Rho, and L. F. Nazar*

*Department of Chemistry, University of Waterloo, Waterloo, Ontario, Canada N2L 3G1*

*Received April 25, 2006. Revised Manuscript Received November 4, 2006*

Ordered mesoporous carbon materials with a semi-graphitized structure have been synthesized by directly employing a tri-block copolymer as a structure directing agent and carbon source to form mesoporous carbon. Poly(ethylene oxide)$_{20}$-poly(propylene oxide)$_{70}$-poly(ethylene oxide)$_{20}$ ($EO_{20}PPO_{70}EO_{20}$), or "P123", was cross-linked in the channels of mesoporous silicate, carbonized, and graphitized. Extraction of the silica produces a mesoporous graphitic carbon replica. The graphitization of carbon was realized by employing transition metals (Fe, Co, Ni) as a catalyst in a reducing atmosphere. Of the three transition metal catalysts, nickel was found to be the best candidate in terms of preserving structural order. All three nanoporous carbon materials have 3 orders higher conductivity and better thermal stability than non-graphitic carbon. A composite of ordered mesostructured carbon/metallic $MoO_2$ (63.7 wt % $MoO_2$) was prepared and examined as a negative electrode in a lithium rechargeable battery. The material exhibited a reversible capacity of 760 mA·h/g in the voltage window 3.0−0.0 V.

## Introduction

Mesoporous carbon materials with high surface area and ordered mesostructures have rapidly attracted growing attention for their potential applications in catalysis, hydrogen storage, and fuel cells and as electrodes in electrochemical devices. Following the report of Ryoo et al. of CMK-1 in 1999,[1] a series of mesoporous carbon materials have been synthesized as the inverse replicas of mesoporous silicates. The silicate structures are formed by growth of soluble silica, templated by either short-chain ionic surfactants to form the MCM-41 and MCM-48 class of mesoporous materials[2] or longer chain tri-block copolymer surfactants to form large-pore silicates first reported by Stucky et al., such as the SBA-15 and SBA-16 silicates.[3] The group members MCM-41 and SBA-15 display a hexagonal mesostructure comprised of linear, hollow silicate tubes, whereas the MCM-48 and SBA-16 structures reflect the gyroidal three-dimensional interpenetrating network of the surfactant assemblies. Carbon precursors impregnated within the hollow cavity of the silicate serve as the sources for the carbon replica mesostructures formed after removal of the silica scaffold.[4]

However, the framework of all the carbon replica materials is inevitably amorphous, which limits their application in electrochemistry because of the relatively low conductivity of amorphous carbon. Developing graphitic mesoporous carbon with higher conductivity is one of the important challenges in this field. In general, high-temperature routes are the conventional way to obtain highly graphitized carbon materials, but such heat treatment inevitably leads to very poorly ordered mesoporous structures.[5] Employing graphitizable carbon precursors and using catalyzed synthesis at low temperatures are two alternatives to high-temperature methods. Some initial work along these lines has very recently appeared. In 2003, Ryoo et al. reported on the preparation of mesoporous carbon with partially graphitic pore walls using acenaphthene as the carbon source impregnated into Al doped SBA-15.[6] Other researchers have introduced a melt impregnation method to synthesize mesostructured carbon with a graphitized structure starting from pitches which have well stacked layers of carbon rings.[7,8] Iron salts were also reported to promote the formation of graphite structures from amorphous carbon.[9]

The methods described above have the important limitation of needing to post-impregnate the silica with carbon precursors, thus adding an additional and intensive process step. Very recently, and simultaneous with ongoing work in our laboratory, Hyeon et al. reported that the polymer template used for silica formation can be utilized to synthesize amorphous carbon mesostructures.[10] Here, we report a convenient in situ synthetic route to obtain graphitized mesoporous carbon directly from the copolymer surfactant P123 ($EO_{20}PPO_{70}EO_{20}$), by employing transition metals as catalysts. As the P123 polymer is the structure directing agent for the silica SBA-15, it need not be removed from the silica

* To whom correspondence should be addressed. E-mail: lfnazar@uwaterloo.ca.

(1) Ryoo, R.; Joo, S. H.; Jun, S. *J. Phys. Chem. B* **1999**, *103*, 7743.
(2) Kresge, C. T.; Leonowicz, M. E.; Roth, W. J.; Vartuli, J. C.; Beck, J. S. *Nature* **1992**, *359*, 710.
(3) Zhao, D.; Feng, J.; Huo, Q.; Melosh, N.; Fredrickson, G.; Chemelka, B.; Stucky, G. *Science* **1998**, *279*, 548.
(4) (a) Jun, S.; Joo, S. H.; Ryoo, R.; Kruk, M.; Jaroniec, M.; Liu, Z.; Ohsuna, T.; Terasaki, O. *J. Am. Chem. Soc.* **2000**, *122*, 10712. (b) Lu, A. H.; Li, W. C.; Schmidt, W.; Kiefer, W.; Schuth, F. *Carbon* **2004**, *42*, 2939.
(5) Fuertes, A. B.; Alvarez, S. *Carbon* **2004**, *42*, 3049.
(6) Kim, T. W.; Park, I. S.; Ryoo, R. *Angew. Chem., Int. Ed.* **2003**, *42*, 4375.
(7) Yang, H.; Yan, Y.; Liu, Y.; Zhang, F.; Zhang, R.; Meng, Y.; Li, M.; Xie, S.; Tu, B.; Zhao, D. *J. Phys. Chem. B* **2004**, *108*, 17320.
(8) Vix-Guterl, C.; Saadallah, S.; Vidal, L.; Reda, M.; Parmentierb, J.; Patarin, J. *J. Mater. Chem.* **2003**, *13*, 2535.
(9) Fuertes, A. B.; Centeno, T. A. *J. Mater. Chem.* **2005**, *15*, 1079.
(10) Kim, J.; Lee, J.; Hyeon, T. *Carbon* **2005**, *42*, 2711.

10.1021/cm060961y CCC: $37.00 
Published on Web 01/03/2007

pores once the replica is formed. Furthermore, its transformation to a graphitic phase is initiated by the impregnated catalyst. We refer to this graphitic carbon material as DGMC. Mesoporous carbon with an amorphous framework directly synthesized in situ from P123 without a catalyst is referred to as DMC. The transition metals (Fe, Co, Ni) were utilized as a catalyst in a 7% $H_2/N_2$ mixture atmosphere.[11]

A feature of highly ordered graphitized porous carbon is that it can serve as a conductive scaffold to encapsulate other materials. This leads to design of structured composites where both components play a role in controlling the characteristics. Only a handful of such carbon-based composite negative materials have been reported including carbon coated silicon nanoparticles[12] and an amorphous carbon/tin/cobalt composite utilized by Sony in their new Nexelion cell. However, these have a very different microstructure than ours reported here based on a core−shell design. A seminal report on tin-filled mesoporous carbon as a negative electrode appeared recently, but here the carbon framework was electrochemically inactive, perhaps as a result of its non-graphitized nature.[13] We chose to use DGMC as a framework to host nanowires of a metallic metal oxide. Along with the interesting properties that such confined systems may exhibit, low valent metal oxides such as CoO, $Co_3O_4$, CuO, and $MoO_{3-\delta}$ have been shown to be promising negative electrode materials in lithium-ion batteries. These electrodes uptake lithium ions (and electrons) by "conversion reactions" that lead to materials consisting of nanometer-scale metallic clusters dispersed in an amorphous $Li_2O$ matrix. The reverse reaction reforms the metal oxide and lithium. Very high capacities are achievable, although an unacceptably high degree of hysteresis is usually seen between oxidation and reduction. A key issue is to restrict crystallite size to nanodimensions to ensure a high degree of reversibility of the reaction. With 20 nm hematite particles, for example, reversible insertion of 0.6 Li per $Fe_2O_3$ is possible, whereas large hematite particles (1 to 2 $\mu$m) undergo an irreversible phase transformation on reaction of only ~0.05 Li. Equally important is inhibiting growth and agglomeration of the metal nanoparticles that are extruded and also ensuring electronic and ionic access of the electrode material. Since graphitic carbon itself is an excellent negative electrode, we sought to use the carbon framework as both an active lithium insertion host and as a restrictive containment system for a complementary negative electrode material, $MoO_2$. This pure metallic oxide shows good capacity for lithium uptake but poor reversibility on cycling. Conversely, the electrochemical properties of the composite material described herein show very good cycling stability. This mesostructured carbon/metallic oxide composite, the first to be reported, takes advantage of the Li uptake properties of both composite components. The graphitic carbon framework serves to constrain the dimensions of the oxide and sustain reversibility of the Li uptake. The $MoO_2$ adds gravimetric capacity to that of the active carbon, and its metallic properties enhance the conductivity. The resultant composite displays promising electrochemical properties including a stable reversible gravimetric capacity of 760 mA·h/g.

## Experimental Section

**Synthesis of DGMC.** SBA-15 was synthesized following a literature method.[14] As-prepared SBA-15 (1.0 g) was dispersed into 5 mL of an aqueous solution containing 0.08 g of $H_2SO_4$, and the mixture was heated at 100 °C for 12 h and 160 °C for another 12 h. The composite was partially carbonized at 550 °C for 6 h in $N_2$. The carbonized nanocomposite was then placed into 8 mL of an aqueous solution of a catalyst precursor based on $FeSO_4$, $CoCl_2$, or $NiSO_4$ (carbon/metal salt = 100:1.5 by molar ratio). The mixture was stirred for 3 h and heated at 100 °C for 12 h, prior to graphitization which was carried out at 900 °C in a 7% $H_2/N_2$ mixture atmosphere for 6 h. To remove the silica in the composite, the sample was soaked in a 10% HF solution. The graphitized mesoporous carbon replica was obtained by centrifugation and then dried.

**Synthesis of DMC.** After dehydration by sulfuric acid, the silica/copolymer nanocomposite was completely carbonized at 900 °C in argon for 6 h. The product, DMC, was obtained by dissolution of the silica with a 10% HF solution.

**Synthesis of Composite DGMC/$MoO_2$.** $MoO_3$ (0.288 g; 0.002 mol; BDH Chemicals, Ltd.) was completely dissolved in 1.5 mL of concentrated ammonium hydroxide solution, and 0.144 g of DGMC (0.012 mol) was added to this transparent solution (C/Mo molar ratio of 6:1). The mixture was sonicated for 1 h until a fine slurry of DGMC/$(NH_4)_2MoO_4$ was obtained. The slurry was heated at 80 °C for 12 h and then under an atmosphere of 7% $H_2/N_2$ mixture at 400 °C for 5 h to obtain the composite material DGMC/$MoO_2$. The percentage (weight) of $MoO_2$ determined by thermogravimetric analysis (TGA) is 63.7%.

**Characterization.** X-ray diffraction (XRD) patterns at low (0.75−4° 2$\theta$) and high angle (10−70° 2$\theta$) were collected on a D8 ADVANCE powder X-ray diffractometer operating at 40 kV and 30 mA and employing Cu K$\alpha$ radiation ($\lambda$ = 0.154 06 nm). Nitrogen adsorption and desorption isotherms were performed employing a Micromeritics Gemini 2735 system at −196 °C. Before measurement, the samples were degassed at 180 °C on a vacuum line overnight. The Brunauer−Emmett−Teller (BET) method was utilized to calculate the surface area. The total pore volume was calculated from the amount adsorbed at a relative pressure of 0.99. The pore size distribution (PSD) was calculated by means of the Barrett−Joyner−Halenda (BJH) method applied to the desorption branch.

The structure of the graphitized mesoporous materials was examined by scanning electron microscopy (SEM) using a LEO 1530 field-emission SEM instrument equipped with an energy-dispersive X-ray (EDX) attachment. Images were recorded at 15 kV with a secondary electron detector. Transmission electron microscopy (TEM) was carried out on a Hitachi HD-2000 operating at 200 keV. TGA of the carbon and composite carbon/$MoO_2$ samples was carried out on a SDT Q600 system in air (5 °C/min; flow, 100 mL/min). The Raman spectra were recorded with a Renishaw 1000 spectrometer using He−Ne laser with the excitation wavelength of 632.8 nm as the radiation source; 25% of the total power (40 mW) was employed for the measurements. Conductivity measurements were performed at room-temperature using the four-

(11) Han, S.; Yun, Y.; Park, K. W.; Sung, Y. E.; Hyeon, T. *Adv. Mater.* **2003**, *15* (22), 1922.
(12) Yoshio, M.; Wang, H.; Fukuda, K.; Umeno, T.; Dimov, N.; Ogumi, Z. *J. Electrochem. Soc.* **2002**, *149*, A15983.
(13) Gigoriants, I.; Sominski, L.; Li, H.; Ifargan, H.; Aurbach, D.; Gedanken, A. *Chem. Commun.* **2005**, 921.
(14) Yu, C.; Fan, J.; Tian, B.; Zhao, D. *Chem. Mater.* **2004**, *16*, 889.

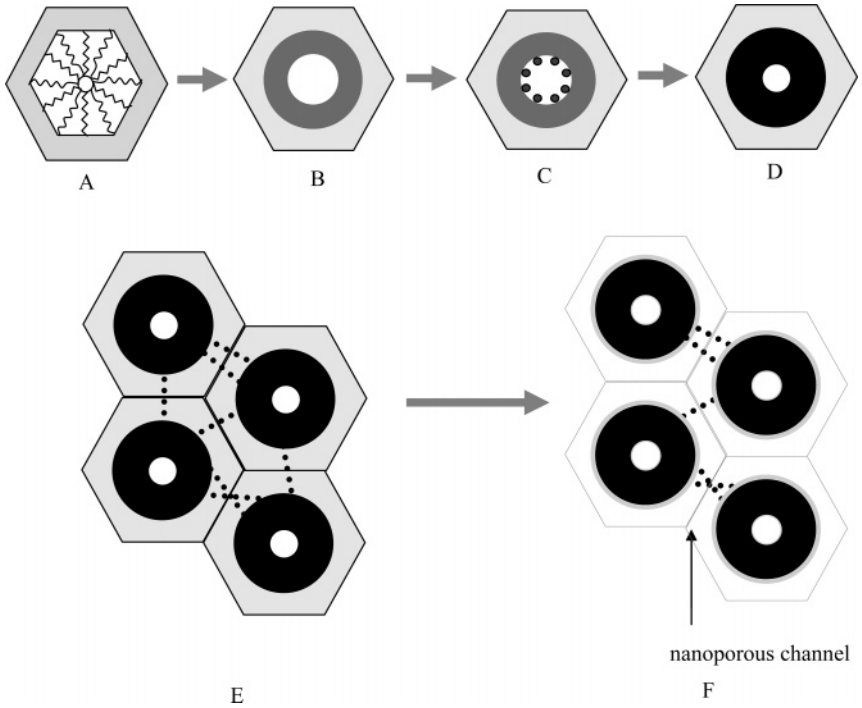


**Figure 1.** Schematic diagram showing the synthesis of DGMC materials: (A) as-synthesized SBA-15; (B) partially carbonized as-synthesized SBA-15; (C) after catalyst loading; (D) after graphitization and complete carbonization; (E) removal of the silica by HF etching showing the carbon fibers that connect the carbon nanorods as dotted lines; (F) graphitized carbon nanorod replica.

point method. Sample bars for the measurement were cut from the pellets and then cold pressed using a force of 44 kN.

**Electrochemical Studies.** Electrochemical evaluation of DGMC/$MoO_2$ was carried out in 2032 coin cells using a commercial (MacPile) multichannel galvanostat/potentiostat operating in galvanostatic mode. A slurry containing 90 wt % composite [DGMC/$MoO_2$ (weight) = 36.3/63.7] and 10 wt % poly(vinylidene fluoride) (PVDF) in cyclopentanone was spread onto a carbon coated copper foil and dried under vacuum overnight at 80 °C prior to punching the electrodes from the current collector. Typical loading of the active mass was between 3 and 6 mg/cm$^2$. The cells were assembled in an argon-filled glove box with oxygen and moisture levels lower than 5 ppm, with an electrolyte composed of a 1 M $LiPF_6$ solution in 1:1 EC/DMC (EM industrials) and lithium metal as the counter electrode.

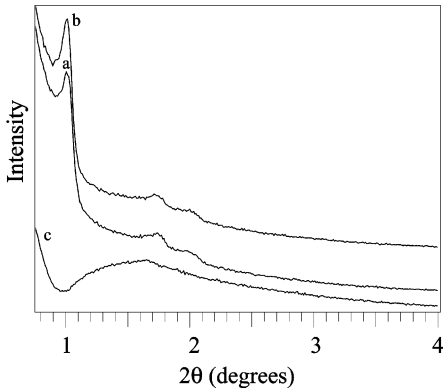


**Figure 2.** Small angle XRD patterns of graphitic nanoporous carbon materials (a) Fe-DGMC, (b) Co-DGMC, and (c) Ni-DGMC.

## Results and Discussion

**(a) Graphitized Carbon Nanorods.** Figure 1 shows a schematic outlining the synthesis route that we employed to create the porous partially graphitized carbon nanorods (DGMCs). SBA-15 with a tubular morphology (rods 1−2 $\mu$m long) served as the template for the DGMC materials. The structure-directing agent, tri-block copolymer P123, was cross-linked in the channels of as-synthesized SBA-15 by dehydration with sulfuric acid and calcination at 550 °C in $N_2$ for 6 h. The channels of the SBA-15 become partially hollow and coated with amorphous carbon.[15] A transition metal $M^{II}$ salt (M = Ni, Fe, or Co) was then impregnated into the carbon-coated channels and reduced to its metallic state in a $H_2/N_2$ atmosphere. These nanoparticles are responsible for catalyzing the graphitization that was activated by a second heat treatment at 900 °C (Figure 1A−D). Because the density of the carbon produced is lower than that of the starting surfactant, the carbon rods have a tubular structure (Figure 1C,D). The silica scaffold is then removed from the structure by dissolution with HF, to yield the partially graphitized carbon replica.

The highly ordered structure of the resultant mesostructured carbon materials Ni-DGMC and Co-DGMC displays well-resolved XRD patterns shown in Figure 2a,b. The reflections are assigned to (100), (110), and (200) reflections of the two-dimensional hexagonal space group (*P*6*mm*), similar to the case of SBA-15. No silica residue could be detected by EDX after etching by HF indicating the long range order is exclusively from the mesoporous carbon replica. There is only a single broad peak in the low angle XRD pattern of the Fe-DGMC sample, which shows that a structure with limited mesostructured order was generated after catalysis with iron nanoparticles (Figure 2c). The carbon materials we obtained are not a collection of carbon fibers but bundles of nanoporous carbon rods with a cylindrical

(15) Zhu, S.; Zhou, H.; Hibino, M.; Honma, I.; Ichihara, M. *Mater. Chem. Phys.* **2004**, *88* 202.

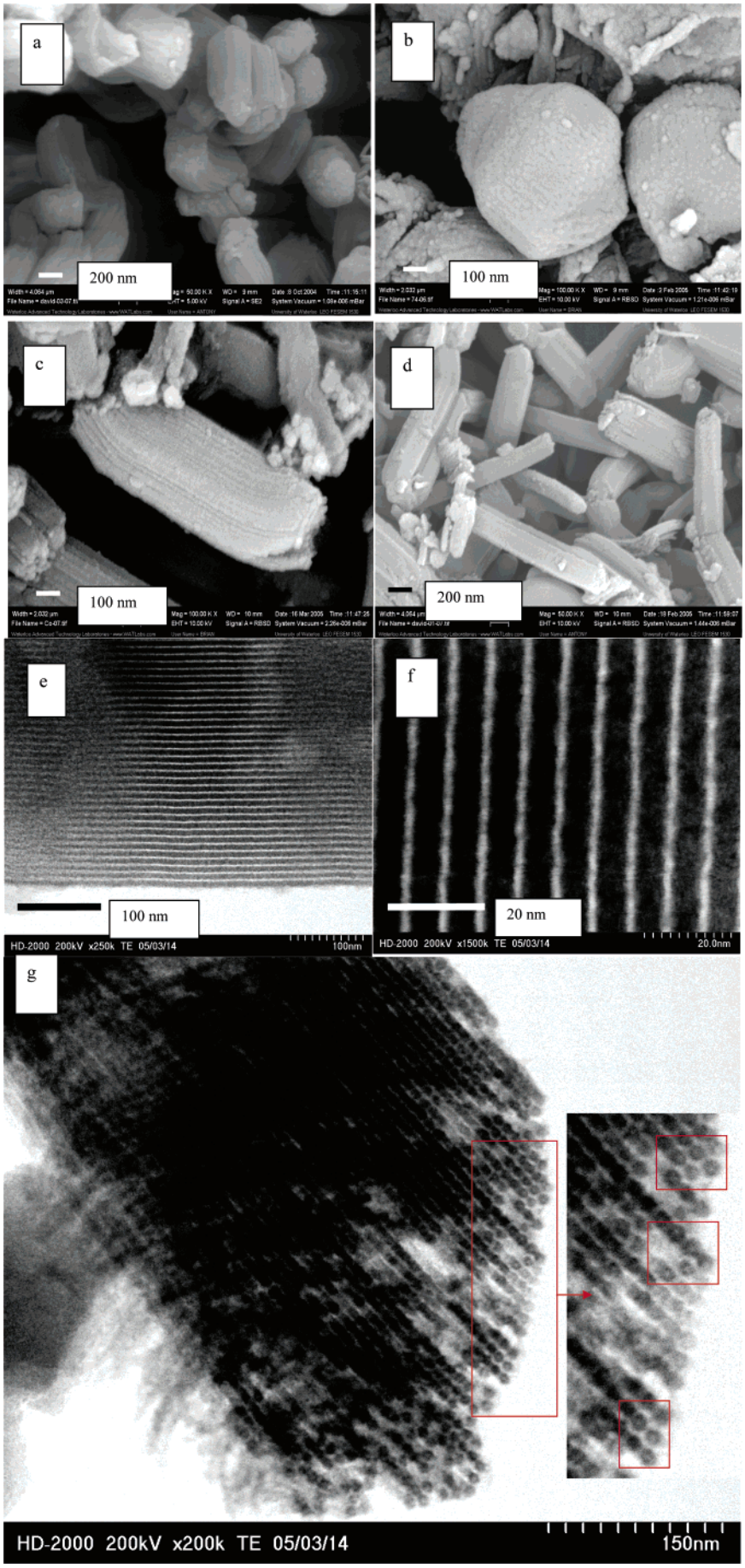


**Figure 3.** SEM images of (a) DMC, (b) Fe-DGMC, (c) Co-DGMC, and (d, e) Ni-DGMC and TEM images of Ni-DGMC: (f) (001) plane and (g and inset) (110) plane. The tubular structure of the rods is indicated by the outlined red squares (inset) in part g.

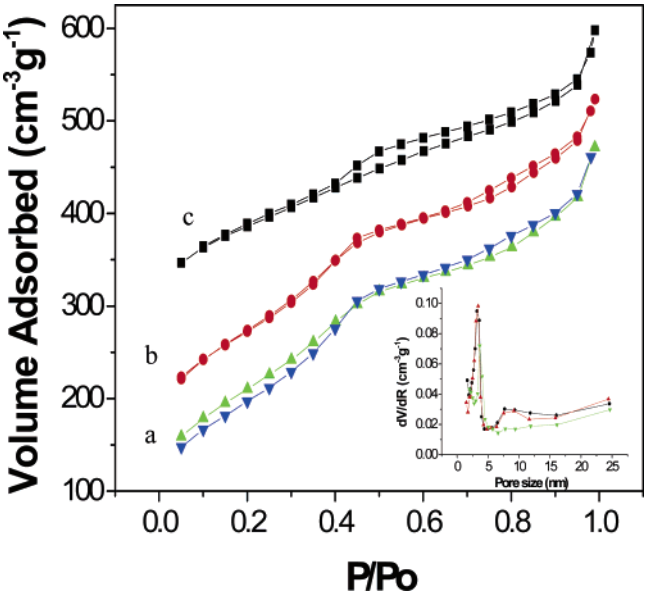


**Figure 4.** $N_2$ adsorption−desorption isotherm for (a) Co-DGMC; (b) Ni-DGMC shifted up by 50 for clarity; and (c) Fe-DGMC shifted up by 200 for clarity. (Inset) PSDs: red, Co-DGMC; black, Ni-DGMC; green, Fe-DGMC.

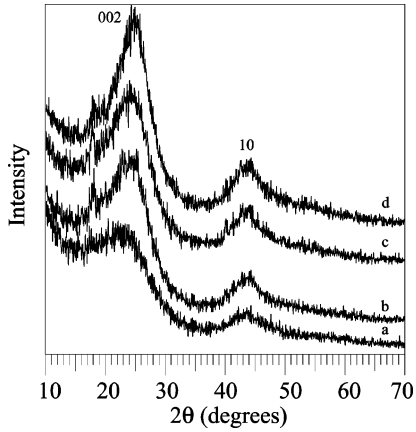


**Figure 5.** Wide angle XRD patterns of (a) DMC; (b) Co-DGMC; (c) Ni-DGMC; and (d) Fe-DGMC. The peak at $2\theta = 18°$ is due to the XRD holder.

hole that runs down their length, whose formation isillustrated in the bottom half of Figure 1. We will provide evidence for this in the following discussion.

SEM and TEM were employed to investigate the morphology and structure of the DGMC materials obtained. The SEM image of DMC (Figure 3a) revealed a rod-like morphology, as did the Co-DGMC and Ni-DGMC materials (Figure 3c,d). This was in contrast to Fe-DGMC, which has an irregular spherical morphology (Figure 3b) and which also displayed the lowest degree of order in the low angle XRD pattern (Figure 2a). A very small fraction of nanoparticles were also apparent on the surface (Figure 3b−d), identified as pure carbon by EDX. They arise from cross-linked polymer, either partially graphitized or amorphous, formed external to the SBA-15 framework. These did not form in DMC itself, which indicates that they are probably produced by catalysis via a minor amount of metal nanoparticles distributed on the surface of the silica−carbon rods. As Ni-DGMC, Co-DGMC, and DMC are all synthesized from the same SBA-15 starting material with the same morphology, the catalyst must control the nature of the final graphitic mesostructure to some degree. For Ni-DGMC and Co-DGMC, we believe that the one-dimensional growth of carbon nanofibers occurs in the channels of SBA-15. This explains why the rods of Ni-DGMC and Co-DGMC are much thinner compared with the amorphous mesoporous carbon DMC rods (Figure 3a). We assume that three-dimensional nucleation and growth processes occur in Fe-DGMC, however, resulting in a lack of well-ordered carbon rod bundles in the SEM image of Fe-DGMC (Figure 3b). The different catalysis mechanisms are related to the different properties of metal catalyst particle surfaces and the intrinsic properties of the metal itself. It is well-known that the orientation of graphite layers of catalytically produced graphite nanofibers (GNFs) can be controlled by the choice of catalyst.[16]

TEM images of Ni-DGMC along two different zone axes, [110] and [001] (Figure 3e−g), clearly show the highly ordered hexagonal mesostructure of the carbon replica, in good agreement with the low angle XRD results. The hollow structure of the rods (i.e., "tubes") can be faintly seen at the edges of the high-resolution image (Figure 3g, indicated by red outlines). The empty channels between adjacent nanoporous tubes are formed by extraction of the SBA-15 silica framework, which has an estimated wall thickness of 3 nm (Figure 3e,f).

BET measurements were carried out on all of the materials. Figure 4 depicts the $N_2$ sorption isotherms of the DGMC materials, and Table 1 summarizes the physical characteristics. All the isotherms show hysteresis at high relative pressures up to 0.95 $P/P_0$, which is not observed in CMK-3 synthesized by completely filling the channels. The capillary condensation of $N_2$ molecules at high relative pressures indicates the existence of another pore system with smaller size and/or structural defects in the carbon walls.[17] The surface areas and pore volumes of DGMC are almost half of their amorphous counterpart, whereas the pore sizes are about the same. The lower surface area of DGMC affirms a well stacked partially graphitized structure which has a higher density than the amorphous carbon materials. The graphitized structure will not support the large fraction of micropores that contribute to high surface areas in amorphous carbon. Fe-DGMC exhibits a high ratio of micropore surface area to the total surface area, indicating the largest amount of structural defects. The primary pore size distribution is

**Table 1. Characteristics of Nanoporous Carbon Materials**

| samples | $S_{BET}$ ($m^2\ g^{-1}$) | micropore surface area ($m^2\ g^{-1}$) | $V_p$ ($cm^3\ g^{-1}$) | pore size (nm) | $d$(002) (Å) | electrical conductivity (S $cm^{-1}$) |
|---|---|---|---|---|---|---|
| SBA-15 (calcined) | 600 | 72 | 0.83 | 7.5 | | |
| DMC | 1800 | 260 | 2.1 | 3.44 | 4.05 | 0.003 |
| Fe-DGMC | 642 | 132 | 0.62 | 3.65 | 3.50 | 1.12 |
| Ni-DGMC | 799 | 69 | 0.73 | 3.23, 7.2 | 3.53 | 1.08 |
| Co-DGMC | 756 | 41 | 0.73 | 3.41,7.2 | 3.55 | 1.63 |

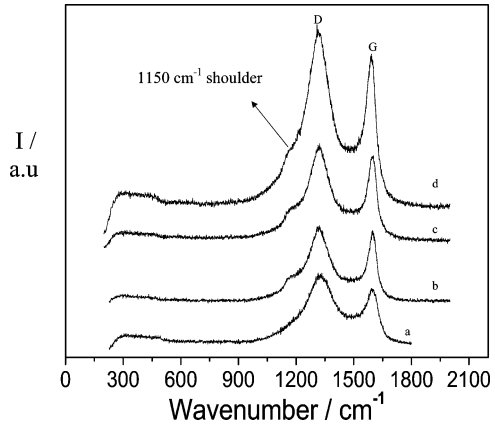


**Figure 6.** Raman spectra of (a) DMC; (b) Ni-DGMC; (c) Co-DGMC; and (d) Fe-DGMC.

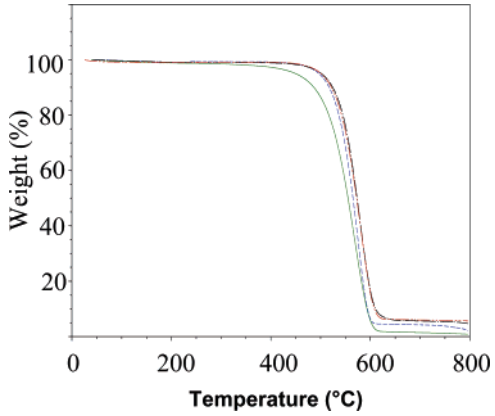


**Figure 7.** TGA curves showing slightly improved thermal stability in air for the graphitized carbon materials: green, DMC; blue, Ni-DGMC; black, Co-DGMC; and red, Fe-DGMC.

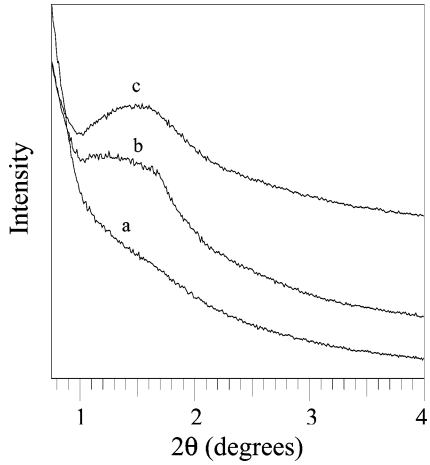


**Figure 8.** XRD patterns of DGMC materials obtained at 1000 °C: (a) Ni-DGMC, (b) Co-DGMC, and (c) Fe-DGMC.

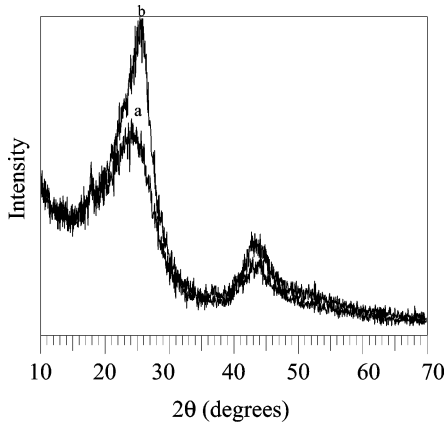


**Figure 9.** XRD patterns of (a) Ni-DGMC at 900 °C and (b) Ni-DGMC at 1000 °C.

bimodal (pore sizes: 3.4 and 7 nm) for the Ni and Co catalyzed DGMCs but is essentially unimodal for the Fe catalyzed sample. It is obvious that the majority of the pore volume with a pore dimension of 3.4 nm is generated from the removal of the silica that forms the original SBA-15 templated structure. These correspond to the channels evident in the TEM image of Ni-DGMC, for example (Figure 3e,f). Pores with a larger diameter are often observed in mesoporous carbon when the carbon filling is not completed by the nanocasting method. The channels are undoubtedly randomly cross-linked with carbon induced by nucleation and growth (Figure 1D,E), as proposed for other mesostructured carbons formed by replica template growth.[18] Such cross-linking would form an ill-defined porous carbon net that is responsible for preventing collapse of the carbon nanowires to a close-packed bundle.

The wide-angle XRD patterns of all of the DGMC materials (Figure 5b−d) exhibit two intense peaks which can be indexed as the (002) and (10) reflections, characteristic of graphitic carbon. The reflections for the DMC carbon are less intense and well defined (Figure 5a), in accord with its much lesser graphitized content. The *d*-spacing of the (002) peak, 0.35 nm, is a little larger than that for graphitized carbon treated at 2800 °C, indicating that the degree of graphitization is limited.[19] The XRD peaks are also not as sharp as graphitic carbon obtained at high temperatures. The semi-graphitic nature of the carbon rods is also very evident in the Raman spectra shown in Figure 6. The G band at 1580 $cm^{-1}$ due to in-plane stretching is noticeably sharper compared with that of non-graphitic DMC (Figure 6b−d). The shoulder at 1150 $cm^{-1}$ is attributed to $sp^2$-bonded configurations in the graphite structure, as proposed in recent work that elucidates the origin of this feature.[20] Among three treated mesoporous carbons, Ni-DGMC has the largest G/D ratio, indicating its higher degree of graphitization.

DGMC exhibits better thermal stability in air than DMC (Figure 7). Mass loss in DMC due to oxidation commenced at 350 °C, while DGMC materials all began to oxidize at ∼470 °C. The conductivity of DGMC materials was in accord with the thermal stability, which is an indirect measure of the graphitic content. The Fe and Co-DGMC exhibited both a slightly higher oxidation temperature and higher conductivity than the Ni-DGMC. Compared with non-

(16) Rodriguez, N. M.; Chambers, A.; Baker, R. T. K. *Langmuir* **1995**, *11*, 3862.
(17) Lin, H. P.; Wong, S. T.; Mou, C. Y.; Tang, C. Y. *J. Phys. Chem. B* **2000**, *104*, 8967.
(18) Choi, W. Ch.; Woo, S. I.; Jeon, M. K.; Sohn, J. M.; Kim, M. R.; Jeon, H. J. *Adv. Mater.* **2005**, *17*, 446.
(19) Mochida, I.; Korai, Y.; Ku, C. H.; Watanabe, F.; Sakai, Y. *Carbon* **2000**, *38*, 305.
(20) Ferrari, A. C.; Robertson, J. *Phys. Rev. B* **2001**, *63*, 121405.

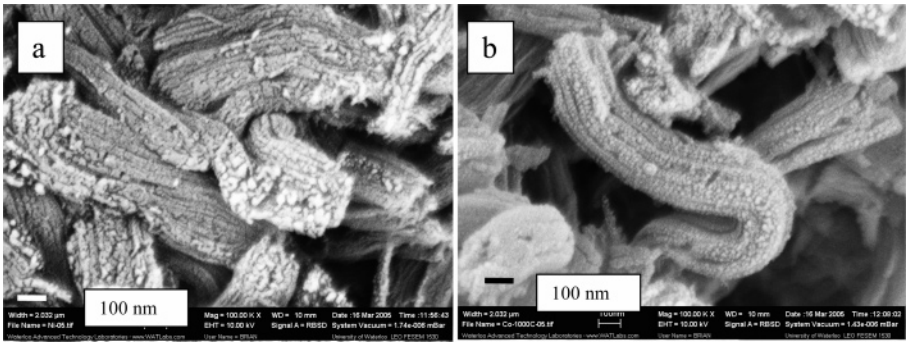


**Figure 10.** SEM images of materials obtained at 1000 °C: (a) Ni-DGMC and (b) Co-DGMC.

graphitic mesoporous carbon, all of the DGMC materials exhibit higher conductivity by almost 3 orders of magnitude (Table 1). The better thermal stability and electric conductivity confirms the graphitic structure of the DGMC materials and has ramifications for materials properties that rely on a more graphitic ordering.

DGMC materials were also synthesized at a higher temperature of 1000 °C. The Ni and Co-DGMC materials give rise to a structure with limited order, indicated by their low angle XRD pattern (Figure 8a,b) and the SEM images (Figure 10). The Ni and Co-DGMC materials obtained at 1000 °C have a much more disordered morphology than the DGMC materials obtained at 900 °C. Interestingly, a broad peak is still present in the XRD pattern of Fe-DGMC (Figure 8c), suggesting that higher temperature treatment does not have such a large influence on Fe-DGMC. On the other hand, the degree of graphitization in the DGMC materials was improved at 1000 °C, illustrated by the increase in the (002) peak and decreased *d* value (0.345 nm) in the XRD pattern of the Ni-DGMC material obtained at 1000 °C compared to the material fired at 900 °C (Figure 9). However, the higher degree of graphitization comes at the expense of partial loss of mesoporous order, as discussed earlier. Therefore 900 °C is an optimum synthesis temperature under these conditions.

**(b) Composite Structure with $MoO_2$.** The composite material was prepared via impregnation of the DGMC catalyzed by Ni with soluble ammonium molybdate, followed by heat treatment in $H_2/N_2$ to reduce the salt to $MoO_2$. The composite composition was confirmed by XRD measurements (see Figure 11) showing reflections of single phase monoclinic $MoO_2$. The line shapes can be deconvoluted into two components: one, highly broadened, that we attribute to the $MoO_2$ confined within the channels, and another which is relatively sharp, suggestive of some $MoO_2$ crystallites >50 nm in diameter that are external to the nanorod surface. These findings were corroborated by TEM studies. The channels of DGMC-$MoO_2$ (Figure 12 a,b) show substantial expansion compared with the nanorods themselves (Figure 12c), indicative of filling of the channels. Note that the carbon rods, which appear dark in Figure 12c due to the contrast between the carbon and the empty tunnel, appear white in Figure 12b in contrast to the higher density $MoO_2$ (dark) that now fills the channels. The metal oxide is relatively continuous along the channel dimension although some disorder of the structure is apparent, vis a vis the DGMC. Some small $MoO_2$ crystallites 30−50 nm in diameter are also evident on the surface of the DGMC rods in Figure 12a, shown by the dark features (indicated by a circled area on the figure) superimposed upon the lattice image. TGA analysis showed that the composites were 63.7 wt % $MoO_2$/carbon (Figure 13).

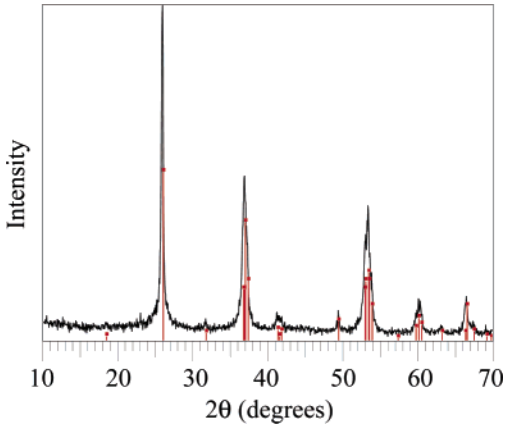


**Figure 11.** Wide-angle XRD pattern of the nanocomposite DGMC/$MoO_2$.

The galvanostatic charge−discharge profiles of the DGMC/$MoO_2$ composite recorded at a current rate of *C*/10 in the 3.0−0.0 V voltage window are shown in Figure 14. The characteristic plateaus representative of crystalline bulk $MoO_2$ are barely visible,[21] confirming the presence of very small nanocrystallites and/or a quasi-amorphous structure.[22] The first discharge sweep yielded a very large specific capacity of 1040 mA·h/g, with an irreversible capacity of 250 mA·h/g (24%) on the first cycle. Figure 15 displays the capacity evolution with cycle number in different voltage windows for the same cell. A reversible, stable charge capacity of 760 mA·h/g was obtained during the first seven cycles in the window 3.0−0.05 V. Raising the lower cutoff voltage to 0.3 V during the subsequent seven cycles decreased the capacity to about 450 mA·h/g, but the initial value of 760 mA·h/g was immediately regained on resetting the cutoff voltage to 0.05 V. The cycling performance was promising, stabilizing at 700 mA·h/g on the 20th cycle. Even better stability was observed when the lower cutoff voltage was maintained at 0.05 V throughout the experiment with very little loss in capacity being observed after 20 cycles.

The very good electrochemical performance arises from two factors. First, both the carbon and the $MoO_2$ contribute

(21) Auborn, J. J.; Barberio, Y. L. *J. Electrochem. Soc.* **1987**, *134*, 638.
(22) Manthiram, A.; Tsang, C. *J. Electrochem. Soc.* **1996**, *143*, L143.

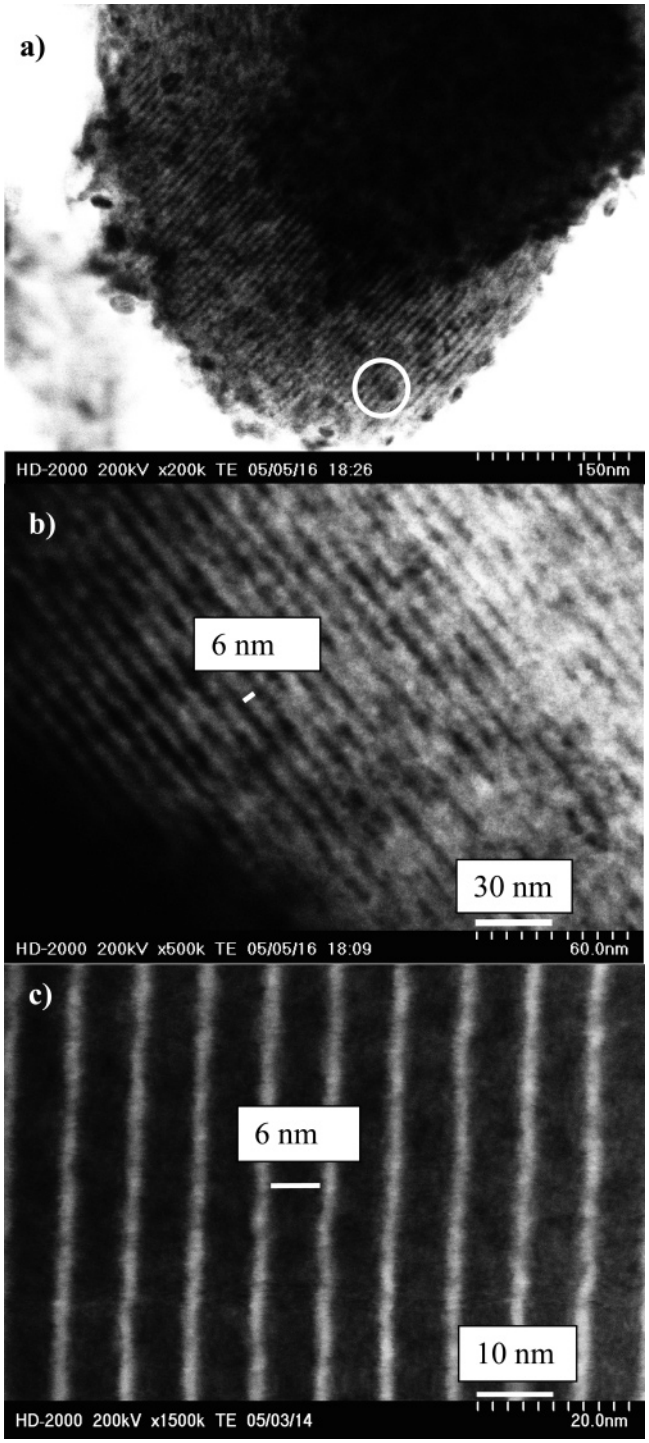


**Figure 12.** TEM images of (a) the nanocomposite DGMC/$MoO_2$ at low magnification showing the stuffed channel structure and presence of a minor amount of $MoO_2$ crystallites external to the DGMC channels; (b) high magnification showing the $MoO_2$ within the channels; (c) "empty" DGMC reproduced from the Figure 3 inset, for easy comparison with part b.

to the capacity of the composite electrode material, according to the proposed reactions:

$$MoO_2 + 4Li \rightarrow Mo + Li_2O \quad (1)$$

$$6C + xLi \rightarrow Li_xC_6 \quad (x \approx 1.0) \quad (2)$$

Here, we assume that full and reversible reduction of $MoO_2$ to Mo metal (+$Li_2O$) occurs within this voltage window, based on previous work reported for metal oxides

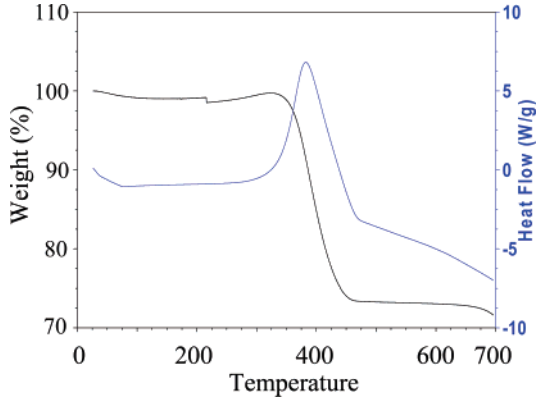


**Figure 13.** TGA curve of the DGMC/$MoO_2$ nanocomposite to determine carbon percentage.

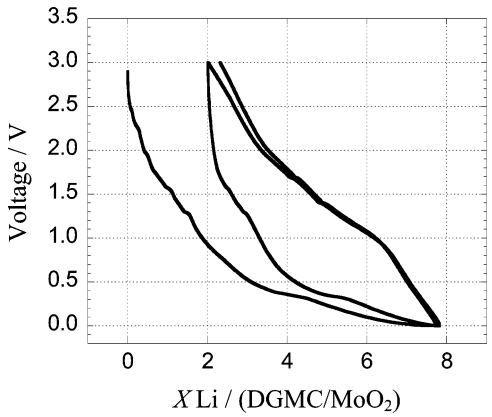


**Figure 14.** Galvanostatic discharge and charge profiles of the first two cycles of DGMC/$MoO_2$.

such as $MoO_3$,[23] CoO,[24] and many others. The DGMC also plays an important role as an active lithium insertion host in the composite electrode. Typical graphitic carbon displays a reversible capacity $Q_r$ of about 370 mA·h/g according to the reaction $6C + Li \rightarrow LiC_6$. The capacity of mesoporous carbon well exceeds this, with values reported as high as 850−1100 mA·h/g for CMK-3.[25] Our DGMC shows a lesser uptake of about 580 to 650 mA·h/g as shown by the first two charge−discharge profiles in Figure 16 and also a correspondingly lower irreversible capacity ($Q_{irr}$) on the first charge sweep. The fraction of reversible capacity (about 30% with respect to the total on first discharge) is the same as CMK-3,[25] however. It is highly characteristic of mesoporous and/or high specific capacity carbons prepared at temperatures <700 °C. It is thought to arise from reaction of lithium with the active surface groups on the carbon, including dangling C−H and C−OH bonds, as well as via formation of the solid electrolyte interface (SEI). As the graphitic character of such carbons increases, either by heat treatment (or by catalysis in our case) both the irreversible and the reversible capacity, and hysteresis in the curve undergoes a dramatic decrease.[25] Accordingly, those parameters for

(23) Leroux, F.; Goward, G. R.; Power, W. P. *Electrochem. Solid-State Lett.* **1998**, *1*, 201.
(24) (a) Poizot, P.; Laruelle, S.; Grugeon, S.; Dupont, L.; Tarascon, J.-M. *Nature* **2000**, *407*, 496. (b) Laruelle, S.; Grugeon, S.; Poizot, P.; Dollé, M.; Dupont, L.; Tarascon, J.-M. *J. Electrochem. Soc.* **2002**, *149*, A627.
(25) Zhou, H.; Zhu, S.; Hibino, M.; Honma, I.; Ichihara, M. *Adv. Mater.* **2003**, *15*, 2107.

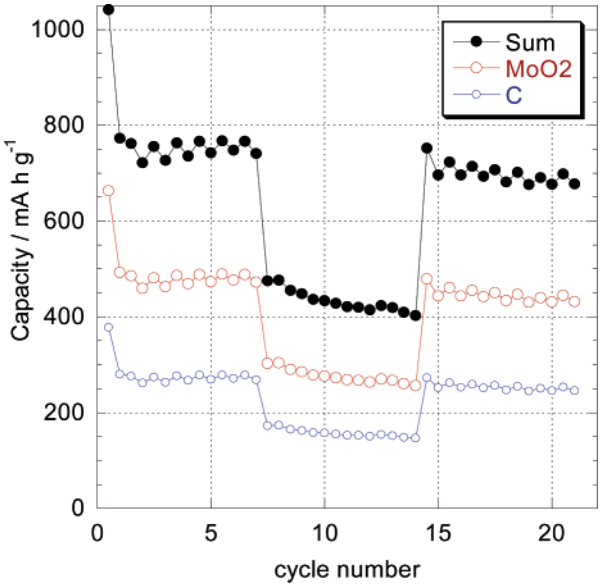


**Figure 15.** Discharge and charge cycle performance of DGMC/$MoO_2$ at a constant rate of C/10; the first seven cycles were recorded in the window 3.0−0.05 V; the lower cutoff voltage was then raised to 0.3 V during the subsequent seven cycles; and the cutoff voltage was then reset to 0.05 V to show the regain in capacity. The contributions of the partially graphitized carbon and $MoO_2$ are estimated as described in the text.

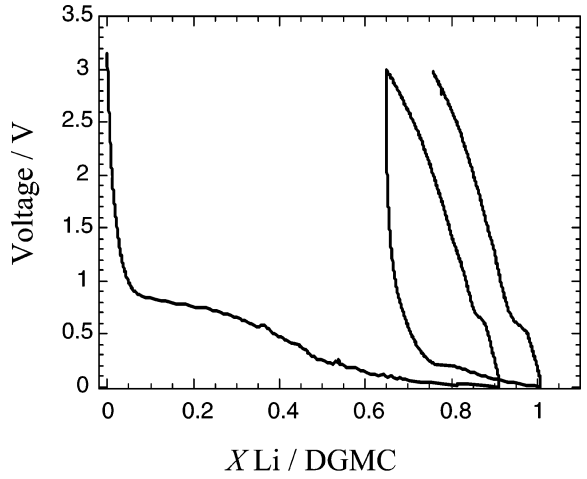


**Figure 16.** Galvanostatic discharge and charge profiles of the first two cycles of DGMC.

DGMC are almost exactly midway between amorphous mesoporous carbon CMK-3 and graphite.

We assume that the capacity of DGMC is the same when it coexists with $MoO_2$ nanoparticles. We note this is contrary to a report of the electrode properties of metallic Sn/mesoporous carbon composites. Those authors did not observe any electrochemical contribution from the carbon even at low potential, possibly due to the amorphous nature of the carbon.[26] Taking into account the 36.3 wt % fraction of mesoporous carbon in our material, the contribution of DGMC in the composite electrode to the overall capacity is about 276 mA·h/g. By this same estimation, the contribution from $MoO_2$ to the overall total capacity of 760 mA·h/g is about 484 mA·h/g, about 58% of the theoretical value (830 mA·h/g) when Mo(IV) is reduced to its metallic state. The breakdown of the components is illustrated in Figure 15. In the composite, in principle, complete Li-driven decomposition of $MoO_2$ is possible because of the small dimensions of the metal oxide nanoparticles, and the intimate contact with the conductive carbon host. That we do not achieve full reduction under our conditions may be due to an overestimate of the carbon contribution and/or hindered transport of Li within the composite structure. In fact, preliminary experiments show that encapsulation of the oxide within three-dimensional hosts such as CMK-8 offers better rate capabilities and higher capacity. However, it is important to note that the composite system described here still presents considerable advantages over the bulk. Crystalline $MoO_2$, which exhibits an average redox potential vs $Li/Li^+$ of 1.3 V, exhibits a monoclinic−orthorhombic phase transition at 1.6 V that leads to very rapid capacity fading if the cell is discharged below this voltage.[21] This is not the case for the composite material, due to the confined, nanosized dimensions of the $MoO_2$. Therefore, not only is more redox capacity accessed, but also the overall voltage is lowered. The pronounced improvement of capacity fading of $MoO_2$ in the DGMC/$MoO_2$ composite is attributable to the controlled particle size of the $MoO_2$. If all of the oxide can be strictly confined in the framework of the mesoporous carbon, even better results are expected. Efforts are underway to achieve this and also to reduce the carbon wall thickness and degree of $MoO_2$ loading within the channels to optimize lithium ion transport. The good electrochemical properties of DGMC/$MoO_2$ indicate that the graphitized mesoporous carbon and transition metal oxide composite materials may be promising candidates to replace graphite anodes in lithium ion batteries.

## Conclusions

We have synthesized highly ordered mesostructured carbon wires with a graphitic structure directly from an as-synthesized SBA-15 silica/triblock nanocomposite, by employing transition metals as catalysts. The graphitic structure can be generated directly from the copolymer in the presence of metallic catalysts based on Fe, Co, or Ni. The catalysts played a major role in determining the morphology of the materials. Enhanced electric conductivity and thermal stability were exhibited by the graphitic nanoporous carbon materials compared with those prepared in the absence of catalyst. A graphitic mesoporous carbon/$MoO_2$ nanocomposite was prepared by a simple impregnation method. Its properties as a negative electrode in a lithium cell, wherein both composite components are active and operate in concert, were evaluated. The graphitic carbon framework serves to constrain the dimensions of the oxide and sustain reversibility of Li uptake. The $MoO_2$ adds substantial gravimetric capacity to that of the carbon which is limited to about 370 mA·h/g (at best), and its metallic properties enhance the conductivity. Thus, forming a nanocomposite with $MoO_2$ gives a synergistic effect: the $MoO_2$ contributes to the two- to threefold

(26) Gigoriants, I.; Sominski, L.; Li, H.; Ifargan, H.; Aurbach, D.; Gedanken, A. *Chem. Commun.* **2005**, 921.

increase in capacity of the composite material as a whole, while the carbon still functions as an active material but also constrains the conversion reaction of the $MoO_2$. This results in a much more stable and reversible capacity of 760 mA·h/g, showing the advantages of this approach in developing nanocomposite electrode materials.

**Acknowledgment.** L.F.N. gratefully acknowledges the NSERC for funding through their Discovery Program and for the award of a Tier 1 Canada Research Chair. The authors greatly appreciate the imaging services provided by the TEM facility at the University of Toronto.

CM060961Y